Vietnam Journal of Earth Sciences, 42(3), 288–297, Doi: 10.15625/0866-7187/42/3/15453

(VAST)

Vietnam Academy of Science and Technology

Vietnam Journal of Earth Sciences

http://www.vjs.ac.vn/index.php/jse

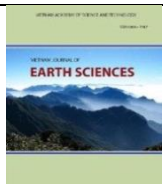

Mapping flood inundation areas over the lower part of the Con River basin using Sentinel 1A imagery

Nguyen Thien Phuong Thao[1,2], Tran Tuan Linh[1], Nguyen Thi Thu Ha[1*], Pham Quang Vinh[3], Nguyen Thuy Linh[1]

[1]*Faculty of Geology, VNU University of Science, Vietnam National University Hanoi*
[2]*Sea and Islands Research Center, VNU University of Science, Vietnam National University Hanoi*
[3]*Institute of Geography, Vietnam Academy of Science and Technology*

Received 15 May 2020; Received in revised form 29 August 2020; Accepted 5 September 2020

ABSTRACT

This study aims to determine a processing method for rapid flood inundation and potential flood-damaged area mapping in the lower part of the Con River basin, a region most vulnerable to floods in Vietnam, using Sentinel 1A (S1A) image. A threshold from -23 dB to -12 dB of the VV band was identified for extracting the water areas from S1A image and was applied in 28 S1A scenes to identify flood dynamics. The time-series map of flood inundation areas during the period of December 2017 to December 2018 evidenced Tuy Phuoc and northern part of An Nhon as the districts most inundated by the 2017 and 2018 floods, which is consistent to the local records. The round-year trend of total flood inundation area shows strong correlations with the Con river water level (R = 0.75) and local precipitation (R = 0.64) measured in Binh Nghi hydro-meteorological station confirming the appropriateness of the study method and the capability of S1A data in monitoring floods.

Keywords: flood; the Con River; inundation; water extraction; sentinel 1A.

1. Introduction

Flood is considered as one of the most frequent and severe natural hazards in the world, causing significant damage to people, infrastructure, and economies. Flood mapping and modeling, therefore, are crucial for flood hazard assessment (Moel et al., 2009), damage estimation (Amadio et al., 2016), and sustainable urban planning (Ran et al., 2016).

Remote sensing, with its advantages of synchronized and frequent observations, has been demonstrated as a promising tool to monitor large-scale floods in a time and cost-efficient manner. Optical satellite imageries, such as MODIS, SPOT, and particular Landsat have been successfully used to delineate flooded areas due to their straightforward interpretability and rich information content (Thenkabail, 2015). However, the inability of optical sensors to acquire clear images during cloudy weather conditions limits its application potential during flood events, which often occur under thick cloud conditions. Microwave remote

*Corresponding author, Email: hantt_kdc@vnu.edu.vn

sensing data, such as Synthetic Aperture Radar (SAR) data can penetrate clouds (Gstaiger et al., 2012; Long, Fatoyinbo & Policelli, 2014) and therefore is considered as an effective tool for flooded area detection (Tholey et al., 2015; Hoque et al., 2011; Henry et al., 2006; Kuenzer et al., 2013). Some high spatial resolution SAR data, such as TerraSAR-X (X-band), COSMO-SkyMed (X-band), and RADARSAT-2 (C-band) (Gstaiger et al., 2012; Pulvirenti et al., 2011), are always expensive which limits the use of the data at large scale. Freely available data, such as ENVISAT ASAR, have a moderate resolution of 150 m, which cannot accurately describe the inter-annual dynamics of the surface water (Kuenzer et al., 2013; Matgen et al., 2011). With the recent launch of the Sentinel-1A (S1A) satellite and the free access to its products (Torres et al., 2012), the S1A data have both high temporal and spatial resolution which can be used to extract surface flooded area and assess its dynamics more efficiently (Cazals et al., 2016).

Although the number of automatic flood mapping approaches has significantly increased over the past years, particular in using S1A data (Plank S, 2014; Twele et al., 2016; Tavus et al., 2018; Olen and Bookhegen, 2018; Ahmed and Kranthi, 2018), a certain amount of manual user interaction is commonly required for satellite data pre-processing, the compilation and adaption of auxiliary data, map production, and the dissemination of derived crisis information to end-users. Additionally, the C-band radar on the S1A offers a high potential for flood mapping due to its enhanced sensitivity of the backscatter signal to open water (Psomiadis, 2016; Kiage et al., 2005; Henry et al., 2006) but it also has noise signals from vegetation coverage within observed region (Olen and Bookhegen, 2018).

Floods were reported in the lower part of the Con River (Binh Dinh province) in recent years to incessant rains, particularly in end-year months of 2017 and 2018 (Tho et al., 2018; Binh Dinh Provincial People's Committee, 2018a). As part of the rapid response, the local disaster management was in urgent need of information about the inundated areas to prioritize their relief and rescue activities. In this study, we employed a simple classification method to map flood inundation areas over the lower basin of the Con River from October 2017 to December 2018 using the S1A data. The method based on a long time series of S1A data was then used to retrieve the flood dynamics at various stages and flood duration. The results on the dynamics of flood and spatial distribution of flood inundation areas over the region during a physical year provide information for better flood mitigation.

2. Materials and methods

2.1. Study area

The lower part of the Con River (also name Kon and Kone) basin located within five districts of Binh Dinh province, including Tay Son, Phu Cat, An Nhon, Tuy Phuoc, and Quy Nhon City (Fig. 1). The study area is located in the downstream of the Con river upon the Thi Nai Lagoon and covers a land area of approximately 1000 km^2 with the average elevation of lower than 20 m above the sea level. The lower part of the Kone River basin has one rainy season, lasting from September to December every year, and one dry season. During the rainy season, rainfall is concentrated and contributes 75–85% to the total annual volume (Phan et al., 2010). Heavy rains often occur in October and November every year, leading to floods and inundations over the study area, particularly in the last

months of 2017 and 2018 (Binh Dinh Hydro-Meteorological Station, 2017a; 2018a). Although Binh Dinh government has many efforts to mitigate flood disasters over the study area in recent years, it is hard to get enough information about flood dynamics and flood inundation state due to the limitation in number and spatial distribution of observation stations. SAR remote sensing may provide information for more effective flood disaster management, overcoming the problem in the ground observation and meeting the needs of local government in integrated flood management of the Con and Ha Thanh river basins (Binh Dinh Provincial People's Committee, 2018b).

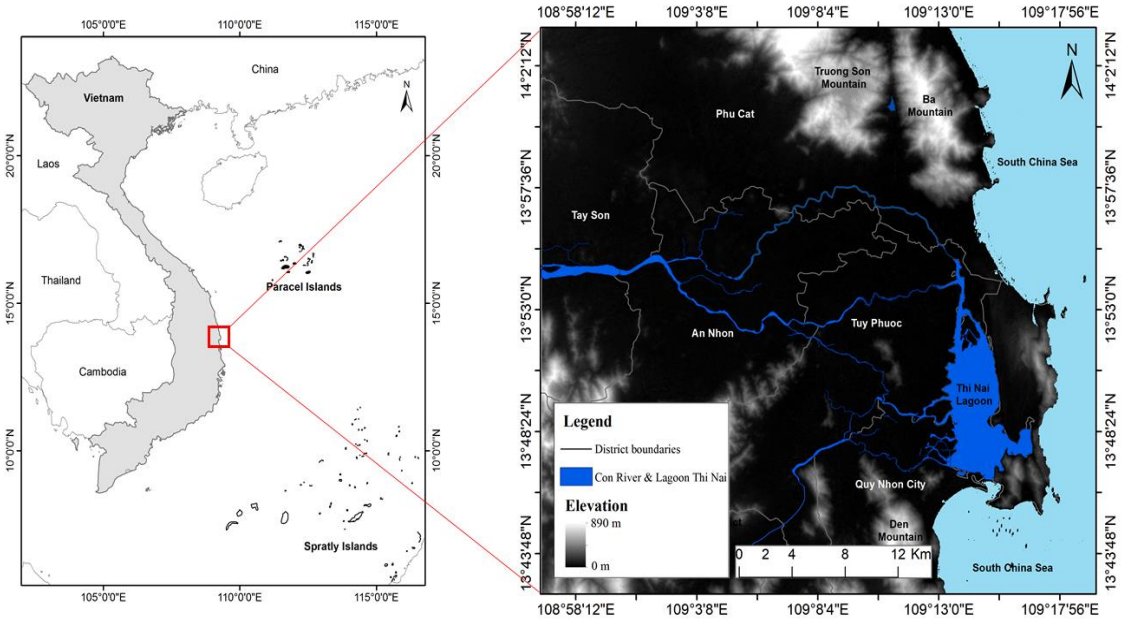

Figure 1. The location of the lower basin of the Con River overlaid the SRTM DEM image with a resolution of 30 m

2.2. Sentinel-1A data processing

In this study, Level-1 Ground Range Detected (GRD) S1A C-band (5.405 GHz) data collected in the Interferometric Wide swath (IW) mode was used which allows the combination of a large swath width (250 km) with a moderate geometric resolution (10 m) and provides ground surface information through dual-polarization bands (VV+VH). A total of 28 S1A images freely available from the European Space Agency (ESA) through Sentinels Scientific Data Hub (https://scihub.esa.int/dhus/), have been used for mapping flood inundation area in the region during the period from October 2017 to December 2018 (Table 1). All downloaded S1A IW GRD products of VV and VH polarization have been processed using the Sentinel Application Platform tool (https://sentinel.esa.int/web/sentinel/toolboxes/sentinel-1) following the flowchart in Fig. 2.

Table 1. Information of S1A images used in this study

No.	Scene Identifier	Acquisition Date
1	S1A_IW_GRDH_1SDV_20171021T223614_20171021T223639_018917_01FF78_3453	21/10/2017
2	S1A_IW_GRDH_1SDV_20171126T223614_20171126T223639_019442_020FC6_FA65	26/11/2017
3	S1A_IW_GRDH_1SDV_20171204T105531_20171204T105556_019552_02132C_5814	04/12/2017
4	S1A_IW_GRDH_1SDV_20180101T223612_20180101T223637_019967_02201F_4031	01/01/2018
5	S1A_IW_GRDH_1SDV_20180113T223612_20180113T223637_020142_0225A8_C9EA	13/01/2018
6	S1A_IW_GRDH_1SDV_20180125T223611_20180125T223636_020317_022B33_559D	25/01/2018
7	S1A_IW_GRDH_1SDV_20180218T223611_20180218T223636_020667_02365E_E57B	18/02/2018
8	S1A_IW_GRDH_1SDV_20180302T223611_20180302T223636_020842_023BEA_2234	02/03/2018
9	S1A_IW_GRDH_1SDV_20180314T223611_20180314T223636_021017_024176_4E6A	14/03/2018
10	S1A_IW_GRDH_1SDV_20180326T223611_20180326T223636_021192_024707_F21C	26/03/2018
11	S1A_IW_GRDH_1SDV_20180407T223611_20180407T223636_021367_024C82_1134	07/04/2018
12	S1A_IW_GRDH_1SDV_20180419T223612_20180419T223637_021542_0251F6_073F	19/04/2018
13	S1A_IW_GRDH_1SDV_20180501T223612_20180501T223637_021717_025778_ABE0	01/05/2018
14	S1A_IW_GRDH_1SDV_20180525T223614_20180525T223639_022067_02629C_6343	25/05/2018
15	S1A_IW_GRDH_1SDV_20180618T223615_20180618T223640_022417_026D7F_3099	18/06/2018
16	S1A_IW_GRDH_1SDV_20180630T223616_20180630T223641_022592_027296_FDD3	30/06/2018
17	S1A_IW_GRDH_1SDV_20180712T223617_20180712T223642_022767_0277CA_C396	12/07/2018
18	S1A_IW_GRDH_1SDV_20180724T223617_20180724T223642_022942_027D4E_39EF	24/07/2018
19	S1A_IW_GRDH_1SDV_20180805T223618_20180805T223643_023117_0282C2_8857	05/08/2018
20	S1A_IW_GRDH_1SDV_20180817T223619_20180817T223644_023292_02886C_7715	17/08/2018
21	S1A_IW_GRDH_1SDV_20180829T223620_20180829T223645_023467_028DFC_5276	29/08/2018
22	S1A_IW_GRDH_1SDV_20180910T223620_20180910T223645_023642_029398_51E2	10/09/2018
23	S1A_IW_GRDH_1SDV_20180922T223620_20180922T223645_023817_029948_D099	22/09/2018
24	S1A_IW_GRDH_1SDV_20181028T223621_20181028T223646_024342_02AA57_0FAC	28/10/2018
25	S1A_IW_GRDH_1SDV_20181109T223620_20181109T223645_024517_02B095_5A58	09/11/2018
26	S1A_IW_GRDH_1SDV_20181117T105538_20181117T105603_024627_02B48B_2DEE	17/11/2018
27	S1A_IW_GRDH_1SDV_20181203T223620_20181203T223645_024867_02BD10_9D39	03/12/2018
28	S1A_IW_GRDH_1SDV_20181215T223619_20181215T223644_025042_02C341_FF19	15/12/2018

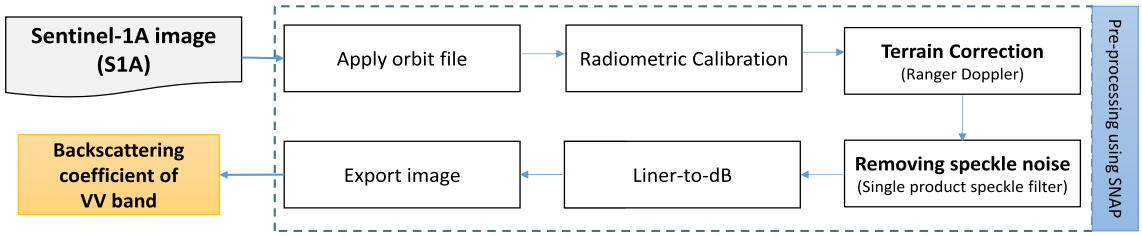

Figure 2. S1A image processing flowchart

2.3. Water extraction method

Mapping flood inundation area from the S1A image means to classify the image into water and non-water areas. In practice, flood inundation areas and/or water areas appear in the SAR images in a dark tone, which can be clearly distinguished from other land surfaces due to a significant difference in surface roughness between them. In this study, the VV-band backscatter (dB), which has been demonstrated the appropriateness for flood detection (Twelve et al., 2016), was explored and used to extract the water areas using the threshold method (Gong et al., 2001). To determine the threshold of the water surface from S1A data, we used the automatic histogram threshold generation method which has been proposed by Zhang et al. (2020). The water areas extracted from S1A image acquired on March 2nd 2018 using this threshold was validated by water areas which were classified from the Sentinel 2A (S2A)

image acquired over the study area on nearly same date (March 4th 2018) (Fig. 3).

The determined threshold of water area in the S1A image was then applied to all 28 S1A scenes to interpret the flood dynamics using a simple density slicing method. It is water areas in the region on March 4th 2018 were classified from the S2A image using the Maximum Likelihood, a supervised classification method, in the routine of the ENVI 5.3 which was proven to be the best method for surface classification using optical data (Sisodia et al., 2014). The inundation area was calculated by the subtraction of during-flood water areas to the pre-flood water areas (Fig. 3).

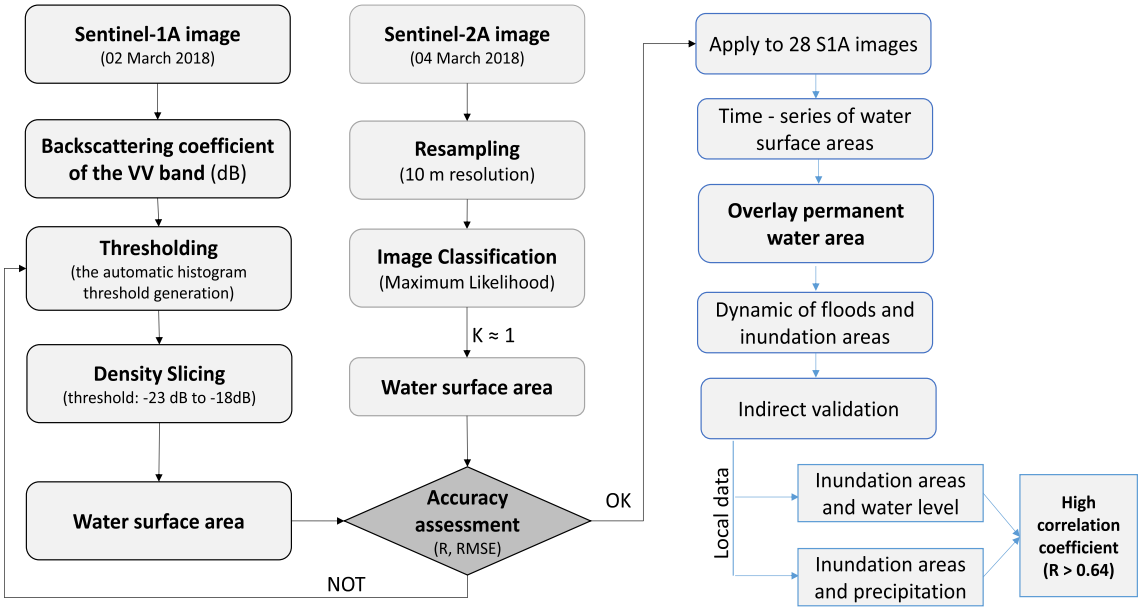

Figure 3. The methodological flowchart for the flood inundation area mapping

2.4. Accuracy assessment

This study used the Kappa coefficient (K) to assess the accuracy of the classification method because it was recognized as a powerful method for analyzing a single error matrix and for comparing the differences between various error matrices (Smits et al., 1999). K is calculated by following equation:

$$K = \frac{P_0 - P_c}{1 - P_c} \quad (1)$$

where is the proportion of units which agree and is the overall accuracy; is the proportion of units for expected chance agreement.

A K of 90% may be interpreted as a 90% better classification than would be expected by random assignment of classes. The general range for K values are if K < 0.4 means a poor kappa value; while, if 0.4 < K < 0.75 is a good kappa value and if K > 0.75 it is an excellent kappa value.

The Pearson correlation coefficient (R) and Root Mean Square Error (RMSE) between water area datasets extracted from S2A and S1A were calculated to evaluate the performance of the determined threshold.

3. Results and discussions

3.1. Spatial distribution of inundation area

The threshold for extracting the water areas from S1A images was determined as from -23 dB to -18 dB through using the automatic histogram threshold generation method for the VV band of the S1A image acquired on March 2nd 2018 as shown in

Fig. 4. Resultant water areas extracted then were compared to the water areas classified from the S2A image acquired on March 4th 2018 by the Maximum Likelihood method with a K value of 0.90 (Fig. 4). Two water area datasets extracted from these both images (S2A and S1A in March 2018) got a high correlation (R = 0.97) and small error (RMSE = 0.57 ha) indicating the excellent performance of the threshold for extracting water area from S1A image. Notably, in some deep-water areas such as lakes and reservoirs in the region, the water area extracted from S1A matched up well (RMSE was lower than 1%) to the water surface zoned form S2A in true color (Fig. 5) confirming the appropriateness of the threshold.

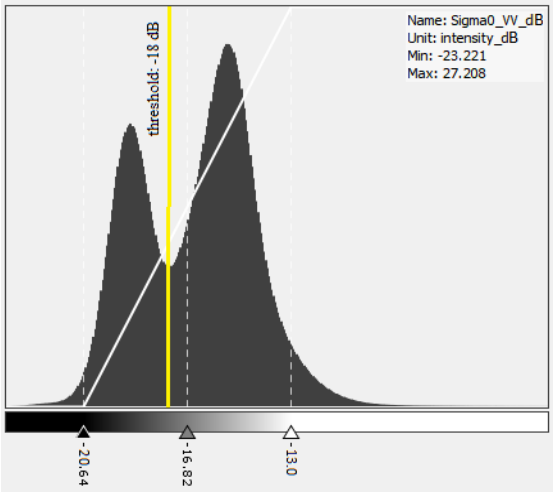

Figure 4. Histogram of backscattering coefficient in the VV band and the illustration of the automatic histogram threshold generation at -18 dB

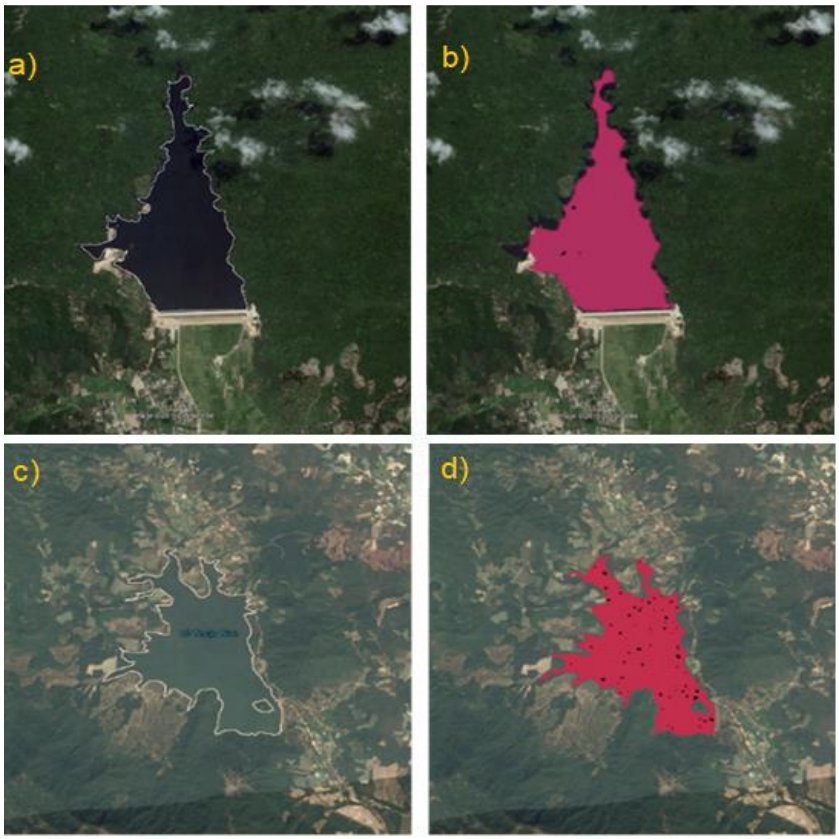

Figure 5. Water surfaces of Nui Mot and Thuan Ninh Reservoirs (Binh Dinh) zoned from S2A image on March 4th 2018 (a and c) and extracted from S1A image on March 2nd 2018 (red areas in b and d) demonstrate the high accuracy of the S1A water surface extraction threshold

Fig. 6 shows the resultant maps of flood inundation areas over the lower part of the Con River basin obtained from 15 S1A scenes those acquired over the area from October 2017 to December 2018. Accordingly, the inundation areas appeared with high density throughout the region in late October to late December of both years 2017 and 2018. In the maps (Fig. 6), Tuy Phuoc district and the northern part of An Nhon district were most affected by floods with total flood inundation area, which reached approximately 20,000 ha in December 2017 and 13,000 ha in December 2018. An Nhon town and Cat Hung commune of Phu Cat district were also affected by floods. According to the maps (Fig. 6), the 2017 flood caused inundation in a larger area than the 2018 flood. The maps also show some areas in Tuy Phuoc district were inundated for nearly 4 months, from late October to the end of January of the next year, as in the 2017 flood. The maps evidence that both floods in 2017 and 2018 caused significant inundation of cropland and rural settlement in the region for more than 3 months, which is consistent with the local report on flood disasters in December 2017 and 2018 (Binh Dinh Provincial People's Committee, 2018a, 2019).

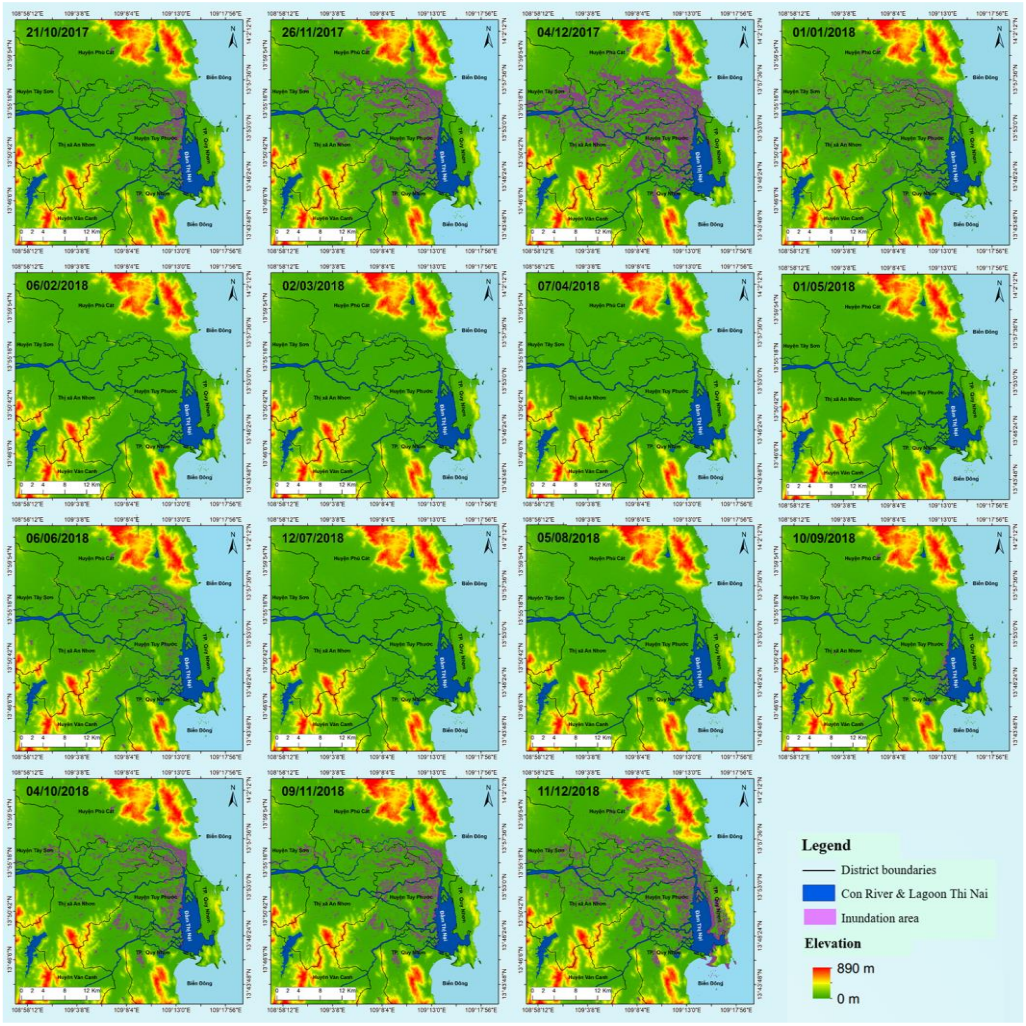

Figure 6. Time-series maps of flood inundation area detected from Sentinel 1A images taken over the lower part of the Con River from October 2017 to December 2018

3.2. Dynamics of floods

One map may help obtain locations of the occasional flood inundation areas only but does not indicate flood dynamics, e.g., when the water level rises. The time-series maps presented in Fig. 6 provide information on the spatial distribution of flood inundation areas, which helps better understand the spatial dynamics of flood in the lower part of the Con River Basin. In order to understand the dynamics of floods, we compared the total flood inundation area detected from 28 S1A images acquired within a physical year-round from December 2017 to December 2018 with the Con River water level and precipitation measured at Binh Nghi hydro-meteorological station (Binh Dinh Hydro-Meteorological Station, 2017b; 2018b) (Fig. 7).

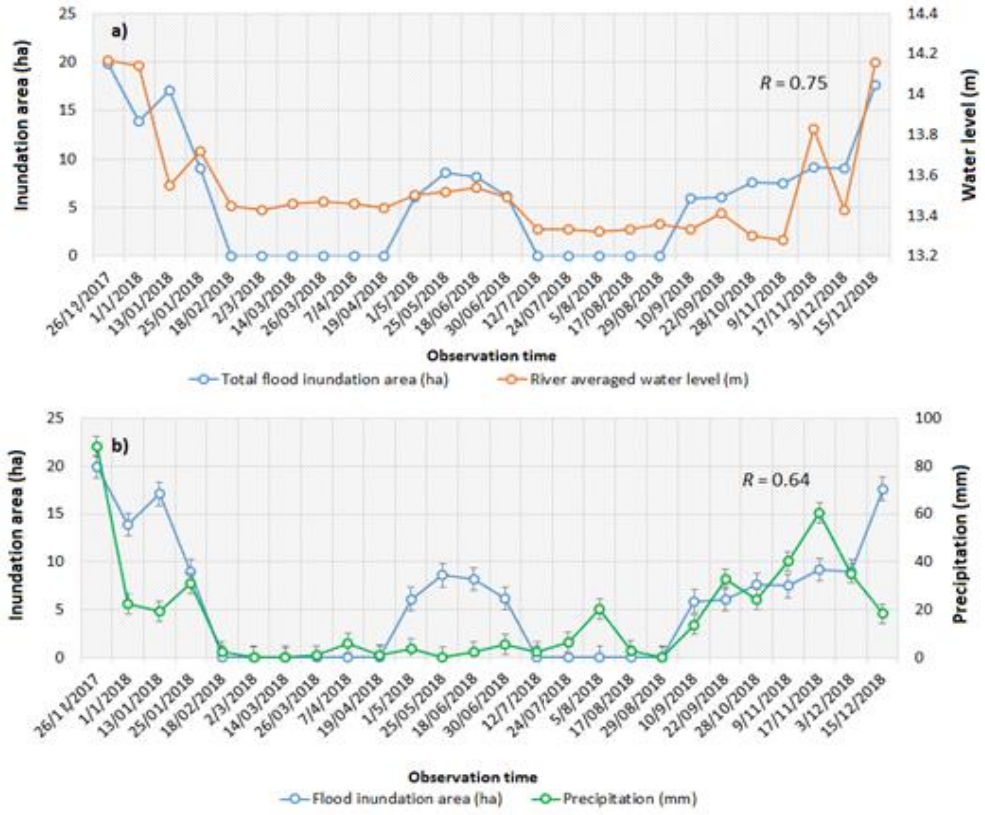

Figure 7. Calibration of the total flood inundation area by comparing with the Con river water level (a) and Precipitation (b) measured at Binh Nghi hydro-meteorological station (Binh Dinh)

The results show that the total flood inundation area is correlated highly to the Con river water level (R = 0.75) and significantly to the precipitation (R = 0.64). In Fig. 7, the total flood inundation area trend shows a good agreement with the Con river water level confirming the high capacity of monitoring flood using S1A images and used methods. The year-round feature of flood inundation area over the region indicates a trend of floods as the following: (1) There are two floods occurred in the lower part of the Con river basin, i.e., one severe flood begins from October and last till to end of January of the next year; the other flood occurs with lower intensity within May and June (Vietnamese

name as "lũ Tiểu mãn"); (2) The strong correlation of the total flood inundation area with the local precipitation (R = 0.64) indicates that the origin of floods is the concentrated water discharge in the rainy season.

The annual flood in the lower part of the Con river basin is the driver of many socio-economic and ecological functions in the region, such as the agricultural production and tourism. Therefore, information on the expected timing and extent of floods is of interest to many stakeholders, particularly local government. Floods can be monitored directly through water levels. However, due to the limited number of monitoring stations over the regions, monitoring of floods can be done using recent satellite images, particularly free SAR data such as S1A. Towards a better management and mitigation of floods in the lower part of the Con River, a map of land-use status in the region should be conducted. Furthermore, an operational monitoring flood over the whole basin should be carried out to provide information for the early disaster warning and management.

4. Conclusions

The work presented here is focused on using S1A SAR data for mapping flood inundation areas over a year period and, therefore, identifying flood dynamics. Based on the results of the study, S1A data demonstrates a great potential in flood inundation area mapping and monitoring with high spatial resolution in a six-day interval. Our analysis showed that the best results in delineating water areas from S1A image were obtained using VV polarization configuration with a threshold of -23 dB to -12 dB. Strong correlations of the total flood inundation area detected from S1A images with the Con River water level (R = 0.75) and local precipitation (R = 0.64) measured at Binh Nghi hydro-meteorological station confirm the appropriateness and validate the use of S1A data to obtain flood inundation area maps with the required accuracy. The results show a trend conforming to the local hydro-climatological feature that flood occurs on the Con river in October every-year and lasts till to the end of January of the next year. Tuy Phuoc district and the northern part of An Nhon district of Binh Dinh province are the most vulnerable to the floods. The proposed methods and data used should be applied to the whole Con River basin for better disaster management over the region.

References

Ahmed C.F., Kranthi N., 2018. Flood vulnerability assessment using geospatial techniques: Chennai, India. Indian J. Sci. Technol, 11(6), 1–13.

Amadio M., Mysiak J., Carrera L., Koks E., 2016. Improving flood damage assessment models in Italy. Nat. Hazards, 82, 2075–2088.

Binh Dinh Hydro-Meteorological Station, 2017a. Flood news in the Con River (Tin lũ trên sông Côn). https://pcttbinhdinh.gov.vn/du-bao-canh-bao/tin-lu-tren-song-kon-1505.html

Binh Dinh Hydro-Meteorological Station, 2017b. Hydro-Meteorological Reports.
https://pcttbinhdinh.gov.vn/du-bao-canh-bao/thong-bao-khi-tuong-thuy-van-thang-10-nam-2018-2827.html

Binh Dinh Hydro-Meteorological Station, 2018a. Flood news in the Con River (Tin lũ trên sông Côn). https://pcttbinhdinh.gov.vn/du-bao-canh-bao/tin-lu-tren-song-kon-21h30-ngay-11-12-3027.html.

Binh Dinh Hydro-Meteorological Station, 2018b. Hydro-Meteorological Reports.
https://pcttbinhdinh.gov.vn/du-bao-canh-bao/thong-bao-khi-tuong-thuy-van-thang-12-nam-2017-1510.html.

Binh Dinh Provincial People's Committee, 2018a. The sumarizing report of disaster prevention and combating in 2017 (in Vietnamese), implementation of tasks in 2018 in Binh Dinh province. Official dispatch No. 139/PCTT dated May 16, 2018.

Binh Dinh Provincial People's Committee, 2019. The sumarizing report of disaster prevention and combating in 2018 (in Vietnamese), implementation of tasks in 2019 in Binh Dinh province. Official dispatch 119/PCTT dated May 17, 2019.

Binh Dinh Provincial People's Committee, 2018b. The decision of approving the outline of tasks of integrated flood management plan in Kon-Ha Thanh river basin. Decision No. 1546/QD-BND dated May 11, 2018.

Cazals C., Rapinel S., Frison P.L., Bonis A., Mercier G., Mallet C., Corgne S., Rudant J.P., 2016. Mapping and characterization of hydrological dynamics in a coastal marsh using high temporal resolution Sentinel-1A images. Remote Sensing, 8(7), 570.

Gong P., Sheng Y., Xiao Q., 2001. Quantitative dynamic flood monitoring with NOAA AVHRR. Int. J. Remote Sens., 22(9), 1709–1724

Gstaiger V., Huth J., Gebhardt S., Wehrmann T., Kuenzer C., 2012. Multi-sensoral and automated derivation of inundated areas using Terra SAR-X and ENVISAT ASAR data. International Journal of Remote Sensing, 33(22), 7291–7304.

Gupta K.K., Gupta R., 2007. Despeckle and geographical feature extraction in SAR images by wavelet transform. ISPRS Journal of Photogrammetry and Remote Sensing, 62(6), 473–484.

Hang P.T.T., Sunada K., Oishi S., Sakamoto Y., 2010. River discharge in the Kon River basin (Central Vietnam) under climate change by applying the BTOPMC distributed hydrological model. Journal of Water and Climate Change, 1(4), 269–279.

Henry J.B., Chastanet P., Fellah K., Desnos Y.L., 2006. Envisat multi-polarized ASAR data for flood mapping. Int. J. Remote Sens., 27, 1921–1929.

Hoque R., Nakayama D., Matsuyama H., Matsumoto J., 2011. Flood monitoring, mapping and assessing capabilities using RADARSAT remote sensing, GIS and ground data for Bangladesh. Nat. Hazards, 57, 525–548.

Kiage L.M., Walker N.D., Balasubramanian S., Baras J., 2005. Application of Radarsat-1 synthetic aperture radar imagery to assess hurricane-related flooding of coastal Louisiana. Int. J. Remote Sens., 26, 5359–5380.

Kuenzer C., Guo H., Huth J., Leinenkugel P., Li X., Dech S., 2013. Flood Mapping and Flood Dynamics of the Mekong Delta: ENVISAT-ASAR-WSM Based Time Series Analyses. Remote Sens., 5, 687–715.

Li K., Shao Y., Zhang F., 2011. Rice information extraction using multi-polarization airborne synthetic aperture radar data. Journal of Zhejiang University (Agriculture and Life Sciences), 37, 181–186.

Long S., Fatoyinbo T.E., Policelli F., 2014, Flood extent mapping for Namibia using change detection and thresholding with SAR. Environmental Research Letters, 9(3), 035002.

Matgen P., Hostache R., Schumann G., Pfister L., Hoffmann L., Savenije H., 2011. Towards an automated SAR-based flood monitoring system: Lessons learned from two case studies. Physics and Chemistry of the Earth, 36(7–8), 241–252.

Moel H.D., Alphen J.V., Aerts J., 2009. Flood maps in Europe–methods, availability and use. Nat. Hazards Earth Syst. Sci., 9, 289–301.

Olen S., Bookhagen B., 2018. Mapping damage-affected areas after natural hazard events using Sentinel-1 coherence time series. Remote Sensing, 10(8), 1272.

Phan T.T.H., Sunada K., Oishi S., Sakamoto Y., 2010. River discharge in the Kone River basin (Central Vietnam) under climate change by applying the BTOPMC distributed hydrological model. Journal of Water and Climate Change, 1(4), 269–279.

Sisodia P.S., Tiwari V., Kumar A., 2014. Analysis of supervised maximum likelihood classification for remote sensing image. In International conference on recent advances and innovations in engineering (ICRAIE-2014), 1–4.

Smits P.C., Dellepiane S.G., Schowengerdt R.A., 1999. Quality assessment of image classification algorithms for land-cover mapping: a review and a proposal for a cost-based approach. International Journal of Remote Sensing, 20(8), 1461–1486.

Van Tho P., Luan N.T., Xuan N.H., Huyen N.T., 2018. Evaluating the impacts of flood to agricultural in Kon-Ha Thanh river basin area, Binh Dinh province base on Radar and GIS. Proceedings of the International Symposium on Lowland Technology (ISLT 2018), Sept. 26–28, Hanoi, Vietnam, 130–137.

Zhang W., Hu B., Brown G.S., 2020. Automatic Surface Water Mapping Using Polarimetric SAR Data for Long-Term Change Detection. Water, 12(3), 872.